

Experimental observation of extremely weak optical scattering from an interlocking carbon nanotube array

Zu-Po Yang,¹ Mei-Li Hsieh,^{1,2,5} James A. Bur,¹ Lijie Ci,³ Leonard M. Hanssen,⁴ Boris Wilthan,⁴ Pulickel M. Ajayan,³ and Shawn-Yu Lin^{1,*}

¹Future Chips Constellation and Department of Physics, Applied Physics and Astronomy, Rensselaer Polytechnic Institute, Troy, New York 12180, USA

²Institute of Electro-Optical Science and Technology, National Taiwan Normal University, Taipei, Taiwan

³Department of Mechanical Engineering & Materials Science, Rice University, Houston, Texas 77005, USA

⁴National Institute of Standards and Technology, Gaithersburg, Maryland 20899, USA

⁵e-mail: mlh@ntnu.edu.tw

*Corresponding author: sylin@rpi.edu

Received 3 February 2011; revised 1 March 2011; accepted 1 March 2011;
posted 1 March 2011 (Doc. ID 142182); published 25 April 2011

We experimentally demonstrate a nearly wavelength-independent optical reflection from an extremely rough carbon nanotube sample. The sample is made of a vertically aligned nanotube array, is a super dark material, and exhibits a near-perfect blackbody emission at $T = 450\text{ K}–600\text{ K}$. No other material exhibits such optical properties, i.e., ultralow reflectance accompanied by a lack of wavelength scaling behavior. This observation is a result of the lowest ever measured reflectance ($R = 0.0003$) of the sample over a broad infrared wavelength of $3\ \mu\text{m} < \lambda < 13\ \mu\text{m}$. This discovery may be attributed to the unique interlocking surface of the nanotube array, consisting of both a global, large scale and a short-range randomness. © 2011 Optical Society of America

OCIS codes: 290.0290, 290.5880, 160.4236.

In emerging energy applications [1–3], there is a renewed interest in finding ways to overcome the fundamental limit of optical reflection from a dielectric surface. For example, in the p-n junction solar cell, optical reflection off the front surface is a practical concern for reaching the Shockley–Queisser limit [4]. In the light-emitting diode (LED), the emitted light is trapped within the so-called light cone [5] and is due to optical reflection at the semiconductor–air interface. The surface microscopic structure offers a new way to reduce reflectance by introducing random surface scattering. Indeed, surface-modified NiP material can have a spectral reflectance of 0.16%–

0.18% in the visible [6]. A surface-roughened LED and solar cell can also improve LED light output [4] and solar conversion efficiency. However, the ultimate goal of achieving near-zero reflection and a nearly perfect optical transmission has not been reached. Furthermore, solar and sensing applications require low reflection over a broad visible and infrared wavelength [7,8]. Conventional black paint has a moderate reflection of 5%–10%. However, in the infrared (5 to 10 μm), its reflectance becomes large, 30%–35%, due to its λ -dependent dielectric constant [9]. A surface-modified NiP material can have a low reflectance in the visible [5], and, yet, its reflectance increases to $\sim 10\%$ at $\lambda = 10\ \mu\text{m}$ [6,10]. A silicon nanotip array can have a low reflectance in the visible [11]. However, its infrared reflectance

increases almost linearly with λ , due possibly to its finite etch depth, a filling fraction (f.f.) of 10%–15%, and a relatively weak surface roughness.

In this paper, we report the discovery of a new type of nanosurface on a vertically aligned carbon nanotube (VA-CNT), exhibiting an ultralow reflectance over a broad wavelength ($\lambda = 3\ \mu\text{m}$ – $13\ \mu\text{m}$). From this realization, we experimentally demonstrate a nearly perfect blackbody radiation from the VA-CNT sample at elevated temperatures, $T = 450\ \text{K}$ – $600\ \text{K}$. We further show a striking discovery of the lowest ever measured reflectance of $R = 0.03\%$ and an apparent breakdown of the λ -scaling behavior of optical reflection by the random CNT surface. We may conclude that, for an extremely rough CNT surface, its optical reflection is dictated by random scattering at different length scales and not by its intrinsic material property.

The VA-CNT samples were prepared by chemical vapor deposition [12] and have a typical film thickness of $500\ \mu\text{m}$. Once grown on a substrate, the film is peeled off by an etching step to obtain a freestanding film [13] and transferred onto a mounting ring, as shown schematically in Fig. 1(a). In Fig. 1(b), we show a side-view scanning electron microscopy (SEM) image of our sample, having a volume f.f. of $\sim 3\%$ [12,14]. Under the mean-field approximation, the sample may be viewed as an array of aligned 1D nanowires with a birefringent index of refraction (S and P). In Fig. 1(c), we show an SEM image of the bottom CNT surface with submicrometer roughness. A schematic of the corrugated surface and optical path of the reflected light are also shown. In Fig. 1(d), we show an SEM image of the top surface of the same

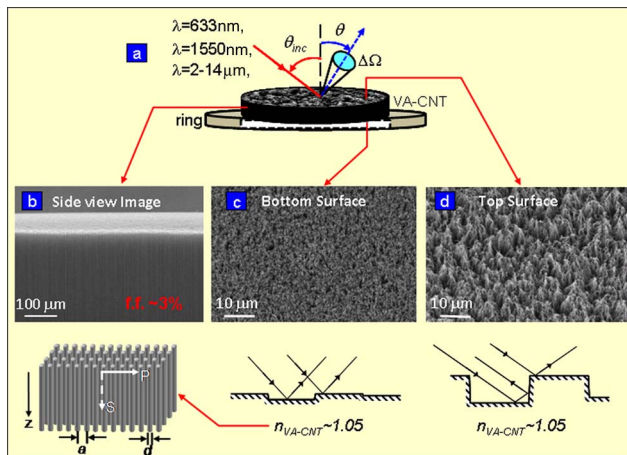


Fig. 1. (Color online) SEM images of vertically aligned CNT samples. (a) A schematic of a freestanding sample, mounted on a ring for ease of testing. Light is incident at an angle θ_{inc} and detected at a different angle θ over the visible and infrared wavelengths. (b) A side-view SEM image of our sample and a schematic of the 1D nanotube alignment. (c) SEM image of the bottom CNT surface with submicrometer roughness. A schematic of light reflection (the arrows) from the surface is shown. (d) SEM image of the top surface of the same sample with a roughness of a few micrometers. A schematic of the light reflection (arrows) from the rougher surface is also shown.

sample with a stronger roughness of a few micrometers (stronger diffuser). Our CNT surface differs from other random surface structures in two major ways. First, the CNT surface consists of interconnected 1D nanowires and not micro- or nanosurfaces. Second, our CNT surface is supported by a low-index VA-CNT structure ($n_{VA-CNT} \sim 1.05$) and not a high-index substrate such as NiP or silicon ($n \sim 3.5$).

We first study the thermal radiation property of our VA-CNT sample and show that it is a nearly perfect blackbody radiator. This is done by comparing radiation spectrum of our VA-CNT to that of a commercial blackbody source. In Fig. 2, we show the measured radiation spectra of a VA-CNT sample (solid curves) and a blackbody source (dashed curves) at $T = 450\ \text{K}$ – $600\ \text{K}$. Previously, a similar measurement was reported for a uniform CNT at a lower temperature of $373\ \text{K}$ and with a moderate reflectivity of 1%–2% [15]. The radiation spectral line shape shown here is a combination of the radiation spectrum from the sample, the detector’s spectral response, and the transmission characteristic of the infrared beam splitter. We noted that the radiation spectra of the CNT sample and the blackbody source are nearly identical for all tested temperatures and wavelengths. Specifically, the emissivity of our CNT sample is found to be $(99 \pm 2)\%$ over the measured infrared wavelengths and for $T = 450\ \text{K}$ – $600\ \text{K}$. Hence, this VA-CNT sample may be viewed as the second kind of a perfect absorber, while the first kind is the well-known “blackbody cavity” first invented over a century ago [16].

By Kirchhoff’s law and in equilibrium, a perfect absorption implies a perfect thermal radiation that follows Planck’s blackbody radiation law [16]. Because both the photonic density-of-states in vacuum and the Bose–Einstein distribution are continuous functions of photon energy, Planck’s radiation is

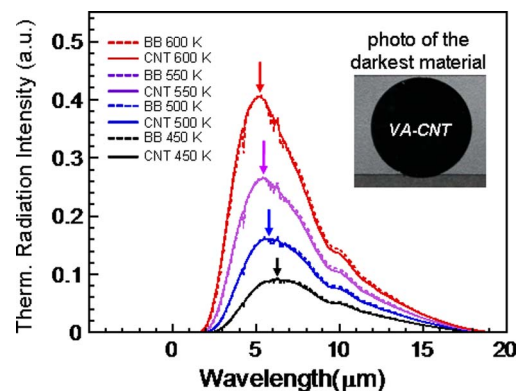


Fig. 2. (Color online) Near-perfect blackbody radiation from a VA-CNT sample. Thermal radiation spectra (solid curves) of our VA-CNT sample taken at elevated temperatures from $T = 450\ \text{K}$ – $600\ \text{K}$. As a reference, blackbody radiation spectra (dashed curves) are also shown. The emission spectra of the CNT sample and the blackbody source are nearly identical for all tested temperatures, indicating that our CNT sample behaves like a nearly perfect blackbody. Inset, photograph of the darkest material made from VA-CNT.

intrinsically a broadband one. Consequently, the experimental observation of a perfect blackbody radiation is a manifestation of both the ultra darkness nature and the broadband nature of our VA-CNT sample.

The demonstration of a nearly perfect blackbody radiation of our VA-CNT prompt us to study its reflection property over a broad infrared range, $\lambda = 3\ \mu\text{m} - 13\ \mu\text{m}$. Some of the reflectance testing was performed at the *National Institute of Standards and Technology*, and the detailed setup is described elsewhere [17]. Briefly, the total and diffused reflectance spectra, $R_{\text{total}}(\lambda)$ and $R_{\text{diff}}(\lambda)$, were obtained by using a combination of an integrating sphere and a Fourier transform infrared spectrometer. The specular reflectance $R_s(\lambda)$ was obtained by subtracting the diffuse from the total reflectance. All measurements were performed at a fixed incident angle ($\theta_{\text{inc}} = 8^\circ$).

In Fig. 3(a), we show the measured reflectance spectra of the bottom CNT surface. As λ is increased from 3 to $13\ \mu\text{m}$, $R_{\text{diff}}(\lambda)$ decreases from 0.0005 to 0.0002 and has a weak λ dependence. Correspondingly, $R_s(\lambda)$ show a strong linear increase, such that $R_s = R_{\text{diff}}$ at $\lambda \sim 5\ \mu\text{m}$ (the vertical dashed line). For $\lambda > 5\ \mu\text{m}$, specular reflectance is larger than the diffused one ($R_s > R_{\text{diff}}$) and the bottom surface

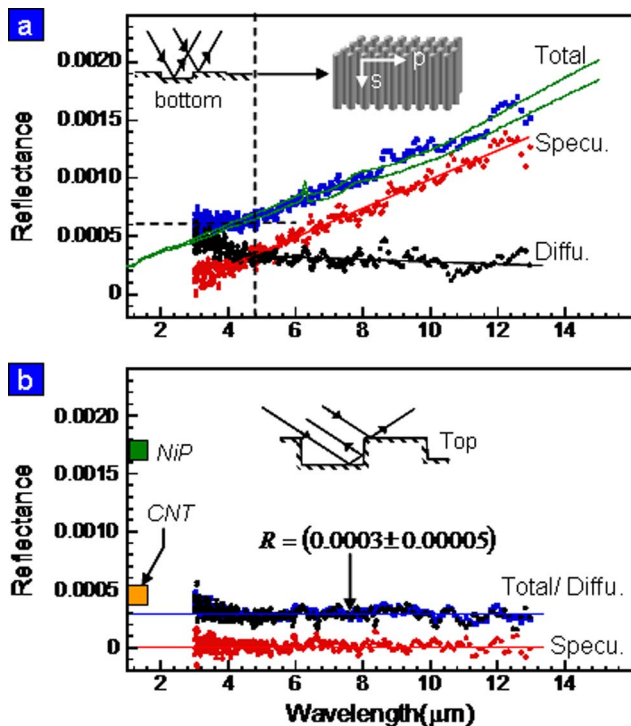


Fig. 3. (Color online) Infrared spectra and scaling behavior of $R_{\text{total}}(\lambda)$, $R_{\text{diff}}(\lambda)$, and $R_s(\lambda)$. (a) The measured $R_{\text{total}}(\lambda)$ (blue squares), $R_s(\lambda)$ (red dots), and $R_{\text{diff}}(\lambda)$ (black dots) from the bottom CNT surface. Both R_{total} and R_s exhibit a strong λ dependent for $\lambda \geq 5\ \mu\text{m}$. In this regime, the CNT surface may be described as a relatively smooth surface, and its reflectance may be modeled (the dashed lines) assuming a slight mixing of p and s polarizations. (b) The measured reflectance spectra from the top surface. R_{total} is nearly λ independent and has an ultralow value of $R_{\text{total}}(0.03 \pm 0.005)\%$ for $\lambda = 4\ \mu\text{m} - 13\ \mu\text{m}$.

becomes a relatively smooth one. Hence, as λ is increased, the dominant optical scattering mechanism switches from been diffused to specular. The observation is consistent with λ scaling and the Rayleigh criterion that a surface is considered to be smooth if it satisfies $\sigma_{\text{rms}} \leq \sigma_{\text{Rayleigh}} = \lambda / (8 \cos \theta_{\text{inc}})$. For $R_{\text{total}}(\lambda)$, the nearly linear λ dependence holds true only for $5\ \mu\text{m} > \lambda > 13\ \mu\text{m}$. There appears to be a λ onset of reflectance at $\lambda \sim 5\ \mu\text{m}$, below which it saturates at $R \sim 0.0006$ (the horizontal dashed line).

The linear λ dependence of $R_{\text{total}}(\lambda)$ for $\lambda > 5\ \mu\text{m}$ may be described by the Fresnel reflection and the Maxwell-Garnett approximation [18–20]. $R_{\text{total}}(\lambda)$ can be calculated assuming a perfectly smooth surface and an effective index, obtained using the index of graphite [21] and a CNT f.f. of 3%. Because the CNTs are not perfectly straight [14], $R_{\text{total}}(\lambda)$ should have contributions from both p and s polarization [see Fig. 1(b)]. At a 99.5%/0.5% P/S mixing ratio, the result of our model calculation shows a good fit to the experimental data for $5\ \mu\text{m} < \lambda < 13\ \mu\text{m}$ [the two green lines in Fig. 3(a) are for a 99.52%/0.48% and 99.48%/0.52% P/S mixing ratio]. The good fit indicates that the smoother bottom CNT surface follows the Fresnel reflection and its λ -dependent reflectance over $5\ \mu\text{m} < \lambda < 13\ \mu\text{m}$ comes from the CNT material's dispersion. Furthermore, from $R_s(\lambda)$ and by the Kirchhoff's theory, the surface roughness σ_{rms} of the sample may be deduced [22,23]. $R_s(\lambda)$ can be written as

$$R_s(\lambda) = R_{\text{smooth}}(\lambda) e^{-4\pi^2 \left(\frac{\sigma_{\text{rms}}}{\lambda}\right)^2 (\cos \theta_{\text{inc}} + \cos \theta)^2}. \quad (1)$$

Here, R_{smooth} is the reflectance of a perfectly smooth surface and σ_{rms} scales linearly with λ . To determine σ_{rms} , we first normalize R_s to R_{smooth} and then plot it as a function " $1/\lambda^2$." In Fig. 4, we show

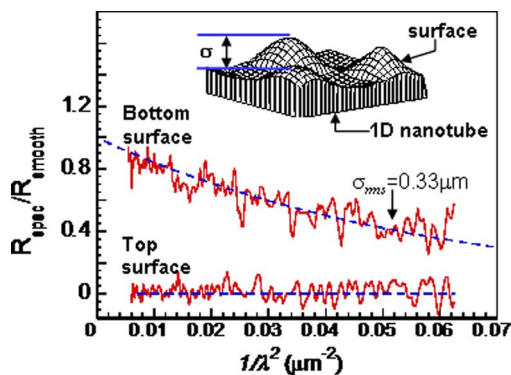


Fig. 4. (Color online) Determination of CNT surface roughness from specular reflectance data. The normalized $R_s(\lambda)/R_{\text{smooth}}(\lambda)$ is plotted versus " $1/\lambda^2$ " (the red curves) for the top and bottom surfaces. For the bottom surface, the fit (the dashed curve) is good using 99.5%/0.5% p/s -polarization ratio and a surface roughness of $\sigma_{\text{rms}} = 0.33 \pm 0.03\ \mu\text{m}$. This roughness is ~ 30 times larger than the nanotube diameter (10 nm). It may be viewed as a global roughness (inset), arising from a random distribution of entangled CNT bundles. For the top surface, we were unable to obtain a meaningful fit due to the negligible $R_s \sim 0$.

the normalized data (the red curves) and exponential fits (the blue curves) for $13\ \mu\text{m} > \lambda > 4\ \mu\text{m}$ or, equivalently, $0.0059\ \mu\text{m}^{-2} < 1/\lambda^2 < 0.062\ \mu\text{m}^{-2}$. The data for the bottom surface can be fitted well using a 99.5%/0.5% *p/s*-polarization ratio for R_{smooth} and a roughness of $\sigma_{\text{rms}} = 0.33 \pm 0.03\ \mu\text{m}$. It is noted that $\sigma_{\text{rms}} \leq \sigma_{\text{Rayleigh}} = \lambda/8 \cos \theta_{\text{inc}}$ for $5\ \mu\text{m} < \lambda < 13\ \mu\text{m}$, and the bottom surface is a relatively smooth one. This σ_{rms} is 30 times larger than a single nanotube diameter of $\sim 10\ \text{nm}$. As shown in the inset of Fig. 4, σ_{rms} may be viewed as a global roughness, arising from a random distribution of entangled CNT bundles. This global surface irregularity of the order of λ could also lead to an enhanced absorption and light-matter interaction [24].

In Fig. 3(b), we show the measured $R_{\text{total}}(\lambda)$, $R_{\text{diff}}(\lambda)$, and $R_s(\lambda)$ taken from the top surface of the same sample. The solid blue and red lines are guides for the eyes. Both R_{total} (blue squares) and R_{diff} (black dots) are exceedingly low, $R_{\text{total}} = (0.030 \pm 0.005)\%$. This value is even lower than the previous lowest reported records of 0.045% [14,18] and 0.16% for NiP [6]. Meanwhile, R_s (the red dots) is negligible. A striking feature of the reflectance data is their λ independence from $\lambda = 3\ \mu\text{m}$ to $13\ \mu\text{m}$, a $\Delta\lambda = 10\ \mu\text{m}$ in the infrared. In contrast, the reflectance of a superblack NiP surface is λ -independent only from $\lambda \approx 2.5\ \mu\text{m}$ to $3.5\ \mu\text{m}$, a $\Delta\lambda = 1\ \mu\text{m}$ [10]. This is a new random scattering regime where specular reflection vanishes completely and diffused reflection dominates and does not have any λ dependence. The data suggest an apparent breakdown of the λ -scaling behavior of optical scattering by the rough CNT surface. To the best of our knowledge, the ultralow R_{total} accompanied by the absence of λ -scaling behavior is a new discovery that has never been reported [10,11,25] before.

It is interesting to note the “bandwidth limit” of the ultralow reflectivity for our nanotube structure. First, at the longer $\lambda > 13\ \mu\text{m}$, such that $\lambda \gg \sigma$, our nanotube surface becomes less rough and would not yield low reflectivity. On the other hand, at the shorter λ limit ($< 200\text{--}300\ \text{nm}$), where $\lambda \gg d$ (nanotube diameter) but $\lambda \sim a$ (distance between successive nanotubes), Rayleigh scattering ($\sim 1/\lambda^4$) from an individual nanotube may dominate and leads to a higher reflectivity.

We comment that the appearance of the λ onset for the bottom surface and the lack of λ dependence for the top surface has never been reported before to our knowledge. It appears that, as one switches from the bottom to the top surfaces, the onset of linear λ dependence was deferred from $\lambda \sim 5\ \mu\text{m}$ to $\lambda > 13\ \mu\text{m}$. Or, as the CNT surface becomes a stronger diffuser, the onset of λ is extended to a longer wavelength. This is a regime where optical reflectance is dominated by a strong scattering off the extremely rough CNT nanosurface.

The influence of CNT roughness on optical reflectance is examined using six different CNT samples with $R_{\text{total}} \cong 0.0009, 0.0007, 0.0006, 0.0005, 0.0004,$

and 0.0003 at $\lambda = 3\ \mu\text{m}$. These samples have nominally the same porous bulk (i.e., the same f.f., optical index, and sample thickness). The difference in their reflectance is presumably due to surface roughness. In Fig. 5, we plot the experimental reflectance as a function of λ . Several points should be noted. First, four samples (surfaces 1–4) show a λ -dependent reflectance with different λ onsets. Second, the decrease in R_{total} from 0.0009, 0.0007, 0.0006 to 0.0005 is accompanied by a shift in the λ onset from 4, 4.4, 5.2 to $5.4\ \mu\text{m}$ (indicated by red vertical lines). Third, the decrease in R_{total} from 0.0009 to 0.0005 is also accompanied by a change in the slope in the nearly linear λ -dependent regime. Finally, the two lowest reflectance samples (surfaces 5–6, $R_{\text{total}} = 0.0004$ and 0.0003 at $\lambda = 3\ \mu\text{m}$) exhibit a very weak, if any, λ dependence. It is noted that another sample with $R_{\text{total}} = 0.00025$ also displays a weak λ dependence. One may assume that R_{total} at $\lambda = 3\ \mu\text{m}$ is a good measure of the degree of CNT roughness. In this case, these data suggest that, for $R_{\text{total}} < 0.0005$ or above a certain critical CNT roughness, optical reflection becomes totally diffused, is extremely weak, and is nearly λ independent. In the inset of Fig. 5(a), the λ onset is plotted as a function of R_{total} . It shows that there seems to be a critical transition at $R_{\text{total}} \approx 0.0005$, where the CNT surface becomes extremely rough and its reflection is nearly λ independent.

At present, there is no satisfactory explanation for all of these observations, particularly for the

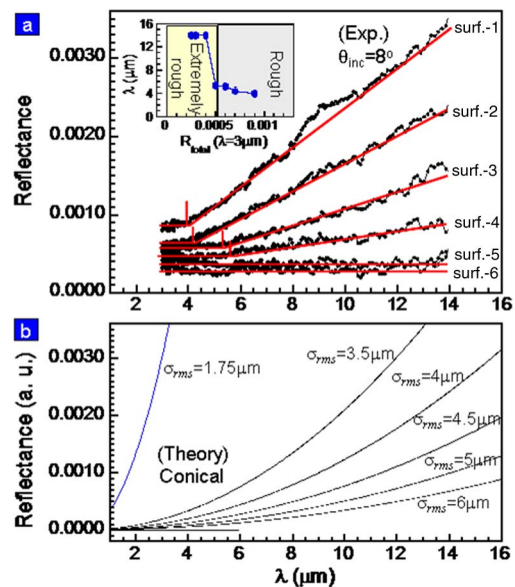


Fig. 5. (Color online) Influence of an extreme CNT roughness on optical reflectance (a) Total reflectance taken from six CNT surfaces with $R_{\text{total}} \cong 0.0009, 0.0007, 0.0006, 0.0005, 0.0004,$ and 0.0003 at $\lambda = 3\ \mu\text{m}$. Four of the surfaces (#1–4) show a λ -dependent reflectance with different λ onsets (indicated by vertical red lines). The two lowest reflectance surfaces (#5–6, $R_{\text{total}} = 0.0004$ and 0.0003 at $\lambda = 3\ \mu\text{m}$) exhibit a weak λ dependence. Inset, the λ onset is plotted versus R_{total} . At $R_{\text{total}} \cong 0.0005$, an abrupt change in the λ onset is observed. (b) The calculated reflectance versus λ for a conical diffuser, having a correlation length $L = 2\ \mu\text{m}$ and a surface roughness $\sigma_{\text{rms}} = 1.75\ \mu\text{m}\text{--}6\ \mu\text{m}$.

λ -independent reflectance at the extremely rough limit [23]. For instance, by the scalar Kirchhoff's theory, the total reflectance of a conical diffuser is given by [26]

$$R \propto \left\{ 1 - \left[1 + \left(\frac{2\pi L/\lambda}{(4\pi\sigma_{\text{rms}}/\lambda)^2} \right)^{-1/2} \right] \right\}. \quad (2)$$

The correlation length L and surface roughness σ_{rms} are expressed in normalized units: " L/λ " and " $\sigma_{\text{rms}}/\lambda$." In Fig. 5(b), we plot the calculated reflectance as a function of λ for $L = 2 \mu\text{m}$ and for $\sigma_{\text{rms}} = 1.75 \mu\text{m} - 6 \mu\text{m}$. In the limit of $\lambda \rightarrow 0$, $(\sigma_{\text{rms}}/\lambda) \rightarrow \infty$, and the reflectance vanishes. At a medium roughness ($\sigma_{\text{rms}} = 1.75 \mu\text{m}$, the blue curve), R increases rapidly with λ . As σ_{rms} is increased ($\sigma_{\text{rms}} = 3.5 \mu\text{m}$ to $6 \mu\text{m}$), the calculated reflectance spectrum decreases accordingly and shows a similar trend as in the series of experimental data in Fig. 5(a). However, all theoretical curves display a monotonic λ dependence, and none of them can reproduce the experimental curves. We understand this result is from a specific model calculation, but there appears to be no satisfactory model for the observed λ onset and the essentially λ -independent reflectance for a broad infrared. As noted earlier, the major difference between conventional rough surfaces and ours is that the CNT surface forms an interlocking nanonetwork consisting of interconnected 1D wires, having a large surface gradient, and not having a well-defined local surface normal. When the surface gradient approaches infinity, the assumption of Kirchhoff's theory breaks down [23,24] and λ -independent reflectance might be possible.

In summary, we experimentally demonstrate the lowest ever reflectance of $R = 0.0003$ and a near-perfect blackbody radiation of $(99 \pm 2)\%$ at $T = 450 \text{ K} - 600 \text{ K}$ from a VA-CNT sample. We show that light reflection from the top CNT surface is essentially λ independent for the entire infrared, $3 \mu\text{m} < \lambda < 13 \mu\text{m}$. We may conclude that the nano-surface reflects little light ($R = 0.0003$), and it acts as a near-perfect absorber and a near-perfect blackbody emitter. This phenomenon is attributed to the multiscale nature of the meshlike surface with a 1D nanotube size of $\sim 10 \text{ nm}$ and a global roughness of 0.3 to $3 \mu\text{m}$. We also believe that our observation should be universally true for other material systems with similar nanosurface and nanostructure. This new class of interlocking nanosurface is ideal for minimizing optical reflection and could have important consequences in maximizing solar energy collection and in the photon extraction of LEDs.

Z. P. Yang, M. L. Hsieh, S. Y. Lin, and J. A. Bur performed the diffuse reflectance profile and thermal emission measurements. L. M. Hanssen, B. Wilthan, Z. P. Yang, and M. L. Hsieh performed the infrared spectrum measurement. L. Ci and P. M. Ajayan contributed VA-CNT samples. S. Y. Lin and M. L. Hsieh designed the experiments, analyzed the data, and

wrote the paper. S. Y. Lin acknowledges financial support from the United States Department of Energy (DOE)—Basic Energy Science under grant DE-FG02-06ER46347.

References

1. Basic Energy Needs for Solar Energy Utilization, Basic Energy Science (U. S. Department of Energy, 2005).
2. Basic Energy Needs for Solid State Lighting, Basic Energy Science (U. S. Department of Energy, 2006).
3. T. J. Coutts, G. Guazzoni, and J. Luther, "An overview of the fifth conference on thermophotovoltaic generation of electricity," *Semicond. Sci. Technol.* **18**, S144–S150 (2003).
4. W. Shockley and H. J. Queisser, "Detailed balanced limit of efficiency of p - n junction solar cells," *J. Appl. Phys.* **32**, 510–519 (1961).
5. I. Schnitzer, E. Yablonovitch, C. Caneau, and T. J. Gmitter, "Ultrahigh spontaneous emission quantum efficiency, 99.7% internally and 72% externally, from AlGaAs/GaAs/AlGaAs double heterostructures," *Appl. Phys. Lett.* **62**, 131–133 (1993).
6. S. Kodama, M. Horiuchi, T. Kunii, and K. Kuroda, "Ultra-black nickel-phosphorus alloy optical absorber," *IEEE Trans. Instrum. Meas.* **39**, 230–232 (1990).
7. R. Takahashi, Y. Saito, Y. Sato, T. Kubo, T. Tomaru, M. Tokunari, T. Sumiya, K. Takasugi, and Y. Naito, "Application of diamond-like carbon (DLC) coatings for gravitational wave detectors," *Vacuum* **73**, 145–148 (2004).
8. M. J. Persky, "Review of black surfaces for space-borne infrared systems," *Rev. Sci. Instrum.* **70**, 2193–2217 (1999).
9. E. A. Taft and H. R. Philipp, "Optical properties of graphite," *Phys. Rev.* **138**, A197–A202 (1965).
10. R. J. C. Brown, P. J. Brewer, and M. J. T. Milton, "The physical and chemical properties of electroless nickel–phosphorus alloys and low reflectance nickel–phosphorus black surfaces," *J. Mater. Chem.* **12**, 2749–2754 (2002).
11. Y. F. Huang, S. Chattopadhyay, Y. J. Jen, C. Y. Peng, T. A. Liu, Y. K. Hsu, C. L. Pan, H. C. Lo, C. H. Hsu, Y. H. Chang, C. S. Lee, K. H. Chen, and L. C. Chen, "Improved broadband and quasisymmetric anti-reflection properties with biomimetic silicon nanostructures," *Nat. Nanotechnol.* **2**, 770–774 (2007).
12. L. Ci, R. Vajtai, and P. M. Ajayan, "Vertically aligned large-diameter double-walled carbon nanotube arrays having ultra-low density," *J. Phys. Chem. C* **111**, 9077–9080 (2007).
13. L. Ci, S. M. Manikoth, X. Li, R. Vajtai, and P. M. Ajayan, "Ultrathick freestanding aligned carbon nanotube films," *Adv. Mater.* **19**, 3300–3303 (2007).
14. Z. P. Yang, L. Ci, J. A. Bur, S. Y. Lin, and P. M. Ajayan, "Experimental observation of an extremely dark material made by a low-density nanotube array," *Nano Lett.* **8**, 446–451 (2008).
15. K. Mizuno, J. Ishii, H. Kishida, Y. Hayamizu, S. Yasuda, D. N. Futaba, M. Yumura, and K. Hata, "A black body absorber from vertically aligned single-walled carbon nanotubes," *Proc. Natl. Acad. Sci. USA* **106**, 6044–6047 (2009).
16. M. Planck, *The Theory of Heat Radiation* (Dover, 1912).
17. L. Hanssen, "Integrating-sphere system and method for absolute measurement of transmittance, reflectance, and absorbance of specular samples," *Appl. Opt.* **40**, 3196–3204 (2001).
18. F. J. Garcia-Vidal, "Metamaterials—towards the dark side," *Nat. Photon.* **2**, 215–216 (2008).
19. F. J. Garcia-Vidal, J. M. Pitarke, and J. B. Pendry, "Effective medium theory of the optical properties of aligned carbon nanotubes," *Phys. Rev. Lett.* **78**, 4289–4292 (1997).

20. J. M. Pitarke and F. J. Garcia-Vidal, "Electronic response of aligned multishell carbon nanotubes," *Phys. Rev B* **63**, 073404 (2001).
21. E. D. Palik and G. Ghosh, *The Electronic Handbook of Optical Constants and Thermo-optic Coefficients* (CD-ROM) (Elsevier, 1999).
22. J. A. Ogilvy, *Theory of Wave Scattering from Random Rough Surfaces* (Hilger, 1991), Chap. 4.
23. P. Beckmann and A. Spizzichino, *The Scattering of Electromagnetic Waves from Rough Surfaces* (Artech, 1987).
24. S. Felix, B. Sapoval, M. Filoche, and M. Asch, "Enhanced wave absorption through irregular interfaces," *Europhys. Lett.* **85**, 14003 (2009).
25. S. R. Meier, "Comparisons of the optical, surface, and constituent properties of morphologically variant black materials," *Proc. SPIE* **5526**, 164–175 (2004).
26. L. G. Shirley and N. George, "Diffuser radiation patterns over a large dynamic range. 1: strong diffusers," *Appl. Opt.* **27**, 1850–1861 (1988).